2013 IEEE/RSJ International Conference on
Intelligent Robots and Systems (IROS)
November 3-7, 2013. Tokyo, Japan

Fish Lateral Line Inspired Hydrodynamic Feedforward Control for Autonomous Underwater Vehicles

Yiming Xu[1] and Kamran Mohseni[2]

Abstract— **Studies have shown that the lateral line found in most fish and some other aquatic organisms is capable of providing hydrodynamic information of the surrounding fluid, which may facilitate many behavioral decisions. Previous work by the group introduced a lateral line inspired feedforward design for underwater vehicle control. The system utilizes pressure sensor arrays to estimate the hydrodynamic force acting on the vehicle such that the additional information will simplify the modeling process and improve the maneuvering accuracy for the control tasks in underwater exploration and environmental monitoring. In this paper, the feedforward control design is presented and tested in simulation for trajectory tracking and path following after expressing the force estimation algorithm in the three-dimensional domain. Pressure measurements at multiple locations on the vehicle surface form a least squares approximation of the pressure distribution. Hydrodynamic forces acting on the vehicle are then estimated and passed to the controller for improved performance. Preliminary experimental tests are conducted to vindicate the proposed algorithm.**

I. Introduction

The lateral line is common to most fish as well as some other aquatic organisms [1], [2]. Studies have shown that it serves an important role in various behaviors including rheotaxis [3], schooling [4], prey detection and capture [5]–[7], and social communication [8]. The neuromasts are the functional units of the lateral line. Specifically, as illustrated in Fig. 1, superficial neuromasts located on the body surface and protruding into the external fluid respond to direct-current and low-frequency components in proportion to the net velocity. Canal neuromasts situated in subdermal canals along the lateral lines respond to high-frequency components, and react proportionally to the net acceleration [7], [9], [10]. Essentially, by detecting water motions and pressure gradients in the surrounding environment, the lateral line system provides hydrodynamic information that may facilitate many behavioral decisions.

To date, several research groups have devoted their efforts to replicating the sensing capabilities of the lateral line. For example, in [11] and [12], designs of micro-fabricated artificial lateral line sensors are tested in dipole flow fields; in [13], pressure sensor arrays are used to identify the flow signature from static and moving cylinders with different cross sections; in [14], parallel arrays of pressure sensors are deployed in the von Kármán vortex street to characterize the hydrodynamic signals for swimming control applications; and in [15], hydrodynamic pressure signals are collected and analyzed on a fusiform-shape craft with forward-backward motions to study the self-motion effects of a fish-like body. In [16] and [17], a biomimetic design of the lateral line system is proposed, which utilizes commercially available pressure sensors to improve the maneuvering accuracy of autonomous underwater vehicles (AUVs) for potential position holding, target tracking, docking, and other control tasks involved in underwater exploration and environmental monitoring.

Traditional control development for underwater vehicles generally considers the dynamics in static flow conditions with perturbation about some nominal traveling speed [18]. Hydrodynamic forces acting on the vehicle are segregated into added mass terms, viscous damping terms, and disturbance terms from the non-static background flow. Based upon the assumption that the vehicle's nominal state of operation remains dominant, the dynamic model can be linearized so that simple online computation may render an effective propulsion command for basic maneuvers. However, advances in high-maneuverability AUVs bring the need for transition among different operation states and performing complex tasks with no dominant state, which requires a better model of the hydrodynamic forces.

Under the heuristic notion that additional knowledge of the dynamics will improve the control performance, sensory information on the background flow may be helpful to achieve the above objectives. In the proposed control structure as illustrated in Fig. 2, a feedforward pathway is introduced to the standard feedback structure, sending signals from the pressure sensors to the controller. Based on the readings, an approximation of the pressure distribution can be obtained. This gives an estimate of the total pressure force acting on the vehicle, which provides information on the added mass, velocity-based damping, and background flow disturbances. Therefore, modeling for the added mass and hydrodynamic damping terms will be unnecessary, and information on the background disturbances is now available so that better control performance may be expected.

The feedforward control design is based on the prototype CephaloBot developed by the group; see [19]. As shown in Figs. 3 and 4, the vehicle is equipped with cephalopod inspired vortex ring thrusters (VRTs) that can provide quantized propulsive force by creating arrays of high-momentum vortex rings with successive ingestion and expulsion of water [20], [21]. This device allows the vehicle to perform accurate maneuvers at low speeds without sacrificing its low-drag streamline profile for efficient high-speed traveling [22]–[24].

[1]Yiming Xu is with Department of Mechanical and Aerospace Engineering, University of Florida, Gainesville, FL 32611 USA `yxu at ufl.edu`

[2]Kamran Mohseni is with Department of Mechanical and Aerospace Engineering, Department of Electrical and Computer Engineering, and Institute for Networked Autonomous Systems, University of Florida, Gainesville, FL 32611 USA `mohseni at ufl.edu`

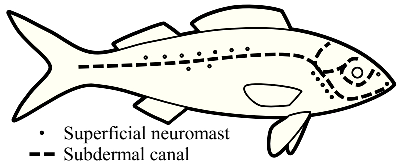

(a) Typical layout of the lateral line in a fish

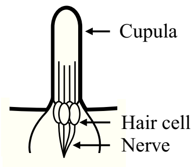

(b) Superficial neuromast

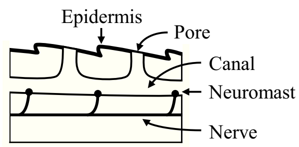

(c) Neuromasts in subdermal canal

Fig. 1. Schematics of the lateral line system in a fish.

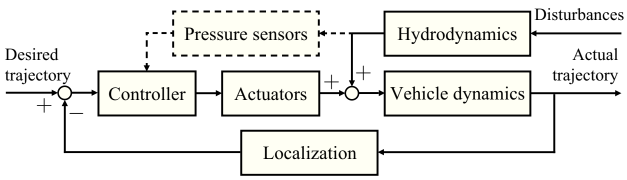

Fig. 2. Block diagram of vehicle control with pressure feedforward.

It is worth mentioning that the feedforward control design described in this paper generally applies to all vehicles, yet it especially suits the need for improving maneuvering accuracy on this particular type of underwater vehicle.

In the following sections, the feedforward dynamic model is given and the force estimation algorithm is expressed in three-dimensional space. Nonlinear controllers with the feedforward are tested in simulation for control accuracy in potential small scale maneuvers as well as long distance cruising. Experimental tests are performed to vindicate the force estimation algorithm.

II. Hydrodynamic Feedforward

A. Dynamic Model

A coordinate system in the body-fixed reference frame is defined as shown in Fig. 4. For motion in the horizontal plane, there are three degrees of freedom, namely, translational motions along x- and y-directions (surge and sway), and rotational motion about z-axis (yaw). At a time instant t, the vehicle's velocity is designated as vector $\boldsymbol{\nu}(t) \in \mathbb{R}^3$. The earth-fixed reference frame is considered to be inertial, in which the earth-fixed coordinate system is defined. Position and orientation of the vehicle can be described in the earth-fixed frame as vector $\boldsymbol{\eta}(t) \in \mathbb{R}^3$. The velocity of the vehicle in the earth-fixed reference frame can be obtained by the following transformation:

$$\dot{\boldsymbol{\eta}} = \mathbf{J}(\boldsymbol{\eta})\,\boldsymbol{\nu}\,, \tag{1}$$

where $\mathbf{J}(\boldsymbol{\eta}) \in \mathbb{R}^{3\times 3}$ represents the transformation matrix.

The dynamic equation for the vehicle can be written in the body-fixed frame as [18]

$$\boldsymbol{\tau} = \mathbf{M}\,\dot{\boldsymbol{\nu}} + \mathbf{C}(\boldsymbol{\nu})\,\boldsymbol{\nu} + \boldsymbol{f}_D + \boldsymbol{f}_N\,, \tag{2}$$

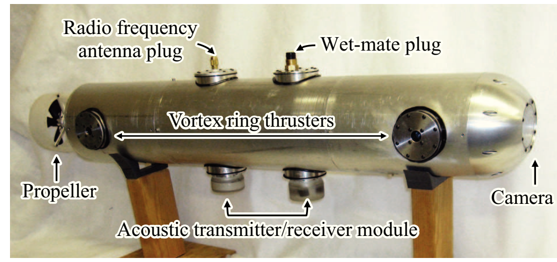

Fig. 3. CephaloBot prototype with cephalopod inspired VRTs.

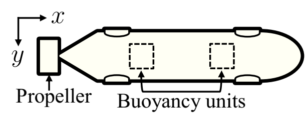

(a) Top view

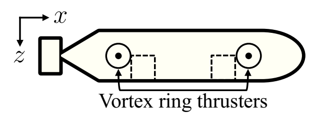

(b) Side view

Fig. 4. Schematics of the propulsion system onboard CephaloBot.

where $\boldsymbol{\tau}(t) \in \mathbb{R}^3$ denotes the vector of control forces and moments from the actuators; matrices $\mathbf{M} \in \mathbb{R}^{3\times 3}$ and $\mathbf{C}(\boldsymbol{\nu}) \in \mathbb{R}^{3\times 3}$ denote the inertial terms and the Coriolis and centripetal terms, respectively; $\boldsymbol{f}_D(t) \in \mathbb{R}^3$ represents the vector of hydrodynamic damping forces and moments; and $\boldsymbol{f}_N(t) \in \mathbb{R}^3$ represents the unmodeled forces and moments.

B. Feedforward Model

According to the feedforward design, the propulsive force $\boldsymbol{\tau}(t)$ combines the feedforward element $\widehat{\boldsymbol{f}}_D(t) \in \mathbb{R}^3$ with a feedback signal $\boldsymbol{\tau}_B(t) \in \mathbb{R}^3$ from any control design

$$\boldsymbol{\tau} = \boldsymbol{\tau}_B + \widehat{\boldsymbol{f}}_D\,. \tag{3}$$

Defining $\widetilde{\boldsymbol{f}}_D(t) \in \mathbb{R}^3$ to be the mismatch between the vector $\boldsymbol{f}_D(t)$ and its estimation $\widehat{\boldsymbol{f}}_D(t)$

$$\widetilde{\boldsymbol{f}}_D = \boldsymbol{f}_D - \widehat{\boldsymbol{f}}_D \tag{4}$$

the equation of motion becomes

$$\boldsymbol{\tau}_B = \mathbf{M}\,\dot{\boldsymbol{\nu}} + \mathbf{C}(\boldsymbol{\nu})\,\boldsymbol{\nu} + \widetilde{\boldsymbol{f}}_D + \boldsymbol{f}_N\,, \tag{5}$$

which presumably reduces the scale of uncertainties in the system as compared with that in (2).

III. Force Estimation

In the body-fixed coordinate system, a biparametric surface describes the boundary of the vehicle. The hydrodynamic damping forces and moments acting on the surface come from the linear and angular velocities and accelerations of the vehicle relative to the background fluid.

Using surface fitting techniques, the pressure readings from sensors at multiple locations can be used to reconstruct the pressure distribution over the entire body. Thus, the total damping force and moment exerted on the vehicle can be estimated by integrating the pressure distribution over the vehicle profile (excluding the locations of the actuators). The resultant force estimation will take the form of linear, fixed weight combinations of the pressure measurements.

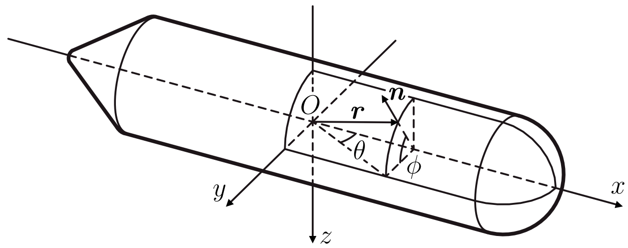

Fig. 5. Geometric model for describing the convex vehicle surface.

A. Vehicle Profile

As illustrated in Fig. 5, the profile of the vehicle is defined in the body-fixed coordinate system. For a point on the vehicle's surface, the position vector $\boldsymbol{r} \in \mathbb{E}^3$ and the normal vector $\boldsymbol{n} \in \mathbb{E}^3$ can be written as

$$\boldsymbol{r} = (r_x,\, r_y,\, r_z)\,, \quad \boldsymbol{n} = (n_x,\, n_y,\, n_z)\,, \tag{6}$$

where r_x, r_y, and r_z are components in $\boldsymbol{r}$ along the x-, y-, and z-axes, respectively; similarly for n_x, n_y, and n_z.

In general, the boundary of the vehicle can be represented with a biparametric surface, and thus, any position on the surface is uniquely defined by specifying a pair of parameters. In this paper, all extruding parts on the vehicle are ignored for simplicity. This gives a convex vehicle surface on which positions are conveniently determined by angles $\theta \in [-\pi,\, \pi) \subseteq \mathbb{R}$ and $\phi \in [-\pi/2,\, \pi/2) \subseteq \mathbb{R}$, as illustrated in Fig. 5. As a result of the parameterization, vectors $\boldsymbol{r}$ and $\boldsymbol{n}$ are expressed as functions in θ and ϕ.

B. Pressure Surface Fitting

Suppose a number of $p = p_\theta\, p_\phi \in \mathbb{N}$ sensors are located on the surface of the vehicle (p_θ and p_ϕ in each corresponding direction). Each sensor takes measurement of the normal pressure $P_s \in \mathbb{R}$ at position $\theta_s,\, \phi_s \in \mathbb{R}$ ($s = 1,\, 2, \ldots,\, p$). Surface fitting over the pressure measurements will give an estimate of the pressure distribution $\widehat{P}(\theta,\, \phi) \in \mathbb{R}$.

A B-spline surface is used to model the pressure distribution due to its flexibility in the spline degree and smoothness, and its linear property that will become helpful for online computation. For $\mathcal{C}^{\,k-2}$ and $\mathcal{C}^{\,l-2}$ continuity in the θ- and ϕ-directions respectively, a closed periodic B-spline surface (see [25], [26]) is used as the approximation function. The estimated distribution $\widehat{P}(\theta,\, \phi)$ can be written as

$$\widehat{P}(\theta,\, \phi) = \boldsymbol{K}_{MN}^{\top}(\theta,\, \phi)\, \mathrm{vec}(\mathbf{B})\,, \tag{7}$$

where $\boldsymbol{K}_{MN}(\theta,\, \phi) \in \mathbb{R}^{mn}$ is the Kronecker product [27] of the vectors of basis functions $\boldsymbol{M}(\phi) \in \mathbb{R}^m$ and $\boldsymbol{N}(\theta) \in \mathbb{R}^n$

$$\boldsymbol{K}_{MN}(\theta,\, \phi) = \boldsymbol{M}(\phi) \otimes \boldsymbol{N}(\theta)\,, \tag{8}$$

the entries in $\mathbf{B} \in \mathbb{R}^{n\times m}$ denote the control vertices of the B-spline surface, and $\mathrm{vec}(\cdot)$ denotes vectorization of a matrix. Further details can be found in [17].

Per surface fitting, the control vertices are approximated in the least squares sense, i.e., for a given set of measuring points, θ_s, ϕ_s, and P_s ($s = 1,\, 2, \ldots,\, p$), the following cost function is minimized:

$$\sum_{s=1}^{p} \Big(\widehat{P}(\theta_s,\, \phi_s) - P_s\Big)^2\,. \tag{9}$$

Substituting (7) into (9) and applying standard linear least squares approximation techniques (refer to [28], [29]) yields m-by-n equations, which in turn can be used to solve for the control vertices $\mathrm{vec}(\mathbf{B})$. Subsequently, the pressure estimation can be expressed as

$$\widehat{P}(\theta,\, \phi) = \boldsymbol{K}_{MN}^{\top}(\theta,\, \phi)\, \mathbf{K}_P\, \boldsymbol{P}\,, \tag{10}$$

in which the matrix $\mathbf{K}_P \in \mathbb{R}^{mn\times p}$ is defined in [17].

C. Estimation Model

Based on the fitting result, the damping force $\boldsymbol{F} \in \mathbb{E}^3$ and moment $\boldsymbol{M}_O \in \mathbb{E}^3$ relative to the origin O acting on the vehicle is estimated by $\widehat{\boldsymbol{F}}, \widehat{\boldsymbol{M}}_O \in \mathbb{E}^3$, which can be written as double integrals over the two-dimensional domain $\mathcal{T} = [-\pi,\, \pi) \times [-\pi/2,\, \pi/2) \subseteq \mathbb{R}^2$

$$\widehat{\boldsymbol{F}} = \iint_{\mathcal{T}} -\boldsymbol{n}\, \widehat{P}(\theta,\, \phi)\, r^2\, \mathrm{d}\theta\, \mathrm{d}\phi\,, \tag{11a}$$

$$\widehat{\boldsymbol{M}}_O = \iint_{\mathcal{T}} -\boldsymbol{r} \times \boldsymbol{n}\, \widehat{P}(\theta,\, \phi)\, r^2\, \mathrm{d}\theta\, \mathrm{d}\phi\,, \tag{11b}$$

where $r = \|\boldsymbol{r}\| \in \mathbb{R}$ is the Euclidean norm of the position vector $\boldsymbol{r}$, and the minus sign comes from the fact that the pressure is considered positive towards the vehicle interior.

For planar motions, the vector of estimated damping forces and moments $\widehat{\boldsymbol{f}}_D \in \mathbb{R}^3$ consists of the forces along x- and y-directions, and the moment about z-axis. Combined with (10) and (11), the force estimate $\widehat{\boldsymbol{f}}_D$ can be expressed as

$$\widehat{\boldsymbol{f}}_D = \iint_{\mathcal{T}} \boldsymbol{b}\, \boldsymbol{K}_{MN}^{\top}(\theta,\, \phi)\, r^2\, \mathrm{d}\theta\, \mathrm{d}\phi\, \mathbf{K}_P\, \boldsymbol{P}\,, \tag{12}$$

where $\boldsymbol{b} \in \mathbb{R}^3$ is defined as

$$\boldsymbol{b} = -\begin{bmatrix} n_x & n_y & r_x\, n_y - r_y\, n_x \end{bmatrix}^{\top}. \tag{13}$$

Using (12), the damping forces and moments are estimated as the pressure signal vector $\boldsymbol{P}$ premultiplied by a constant matrix, once the locations for the sensors are fixed. Since only matrix multiplication is required for online calculation, the force estimation can be rendered rapidly by the onboard embedded system.

IV. Control Simulation

Control simulations are carried out to examine the performance of the hydrodynamic feedforward design. Trajectory tracking under various localization errors is investigated for maneuver accuracy, and path following under constant background flow is tested for control performance in potential long distance traveling. The desired trajectory in the former test includes orientations and the controller is to utilize all available actuators to minimize the tracking error, whereas in the latter test the controller will be focusing on orientating the vehicle towards the desired positions and mainly relying on the rear propeller for locomotion.

TABLE I
COMPARISON OF CONTROL PERFORMANCE FROM 20 TO 60 S

	Units	Without pressure feedforward		With pressure feedforward	
		Mean	Maximum	Mean	Maximum
Absolute	m	1.403	3.692	1.171	2.084
position	m	1.832	4.026	0.929	1.815
error	rad	0.408	1.464	0.298	0.606
Absolute	m/s	4.654	12.582	2.806	5.758
velocity	m/s	1.902	6.914	1.411	3.584
error	rad/s	1.139	6.132	0.843	2.006
Absolute	N	152.909	300.000*	40.441	217.375
control	N	100.584	300.000*	20.292	134.517
input	N·m	15.953	86.813	5.926	28.032

* The control input reaches the saturation level.

A. Hydrodynamic Model

In this simulation, a two-dimensional hydrodynamic model is developed using the potential flow theory and is then extended to the three-dimensional space to provide a reference pressure distribution over the vehicle surface.

To simplify the hydrodynamic calculation, an elliptic body is used to represent the vehicle on the horizontal plane, around which the flow is estimated by the potential flow theory, assuming the flow to be irrotational, incompressible, and inviscid. The Kutta condition is applied at the rear end of the ellipse to account for the sharp corner where the vehicle's propeller is located.

For positions on the horizontal plane, the pressure values come directly from the hydrodynamic calculation on an ellipse that represent the vehicle. The pressure value at a location off the plane is assumed to be the projection length of the normal pressure vector. Examples of similar techniques can be found in [30], [31].. It should be noted that even though the hydrodynamic calculation may be inaccurate in terms of representing the realistic background fluid, the simulation tests are still valid for investigating the idea of using hydrodynamic force estimation to improve control performance.

B. Trajectory Tracking

In this simulation, the inertia matrix $\mathbf{M}$ is expressed as

$$\mathbf{M} = \begin{bmatrix} p_1 & 0 & 0 \\ 0 & p_1 & p_2 \\ 0 & p_2 & p_3 \end{bmatrix}, \tag{14}$$

with parameters $p_1, p_2, p_3 \in \mathbb{R}$ defined to be

$$p_1 = 20 \text{ kg}, \quad p_2 = 2 \text{ kg}\cdot\text{m}, \quad p_3 = 4 \text{ kg}\cdot\text{m}^2. \tag{15}$$

The desired trajectory $\boldsymbol{\eta}_d(t) \in \mathbb{R}^3$ is designated as

$$\boldsymbol{\eta}_d(t) = \begin{bmatrix} 5\sin(0.15\,t) & \text{m} \\ 5 - 5\cos(0.15\,t) & \text{m} \\ 0.15\,t + 0.06 & \text{rad} \end{bmatrix}, \tag{16}$$

which represents a horizontal circular orbit with a radius of 5 m, and a time period of about 42 s.

Assume the hydrodynamic estimation mismatch and unmodeled terms to be $\mathcal{C}^2$ continuous and upper bounded by known constants. The control design is based on the 'robust integral of the sign of the error' (RISE) technique (see [32]–[34]) to accommodate the unknown disturbances, in conjunction with backstepping (refer to [35]) to bridge the control design between the reference frames.

During the simulation, the localization error is accounted for with a combination of dead band zones and sinusoidal noise in the position and velocity measurements. The control performance between the time interval from 20 to 60 s in one of test is summarized in Table I. Due to the measurement noise, the controller is unable to acquire the actual tracking error. The tracking error is confined within some intervals governed by the magnitudes of the noise and the control gains. However, since the system with the feedforward is able to counteract the hydrodynamic forces, better control performance may be achieved, as it agrees with the simulation result. It is also worth noticing that less control effort may be needed with the feedforward for the same task.

C. Path Following

The same dynamic model is used for this test. Unlike the desired trajectory in (16), the desired path is defined as a vector $\bar{\boldsymbol{\eta}}_d(t) \in \mathbb{R}^2$ of positions inside the horizontal plane

$$\bar{\boldsymbol{\eta}}_d(t) = \begin{bmatrix} 10\cos(\pi\,t/60) & \text{m} \\ 5\sin(\pi\,t/30) & \text{m} \end{bmatrix}, \tag{17}$$

which traces a figure of eight with a time period of 120 s.

In the body-fixed frame, each component in the control input $\boldsymbol{\tau}(t) = [\tau_x(t),\, \tau_y(t),\, \tau_{oz}(t)]^\top$ is designed separately. The control force τ_x is defined to minimize the position error along x-direction, the torque τ_{oz} is defined to align the vehicle to the desired orientation in order to reduce the tracking error, and the force τ_y is to compensate the sideslip motion caused by τ_{oz} (due to the nonzero parameter p_2). In effect, the control strategy resembles that of the underactuated vehicles where the propeller controls the speed and the rest of the actuators are responsible for the steering. Since the front of the vehicle tends to face the incoming flow rather than the side of the vehicle moving against the fluid, the path following method is potentially more energy efficient compared to that in the previous test for long distance traveling.

Shown in Fig. 6(a) is the trajectory of the vehicle following the path under static background environment starting from the initial state $\boldsymbol{\eta}(0) = \begin{bmatrix} 8 \text{ m} & 0 \text{ m} & 0 \text{ rad} \end{bmatrix}^\top$. The tracking error with and without hydrodynamic feedforward in constant flow (at a speed of 0.35 m/s along y-direction in the earth-fixed frame) is shown in Fig. 6(b) and (c), respectively. Due to the lack of sway actuation, the path following error cannot be eliminated especially with the unsteady background flow. However, the feedforward controller is able to reduce the path tracking error by adjusting the vehicle orientation according to the estimated hydrodynamic forces.

V. EXPERIMENTAL TESTS

The force estimation algorithm is tested in experiment. In the setup shown in Fig. 7, an upright cylinder is rigidly

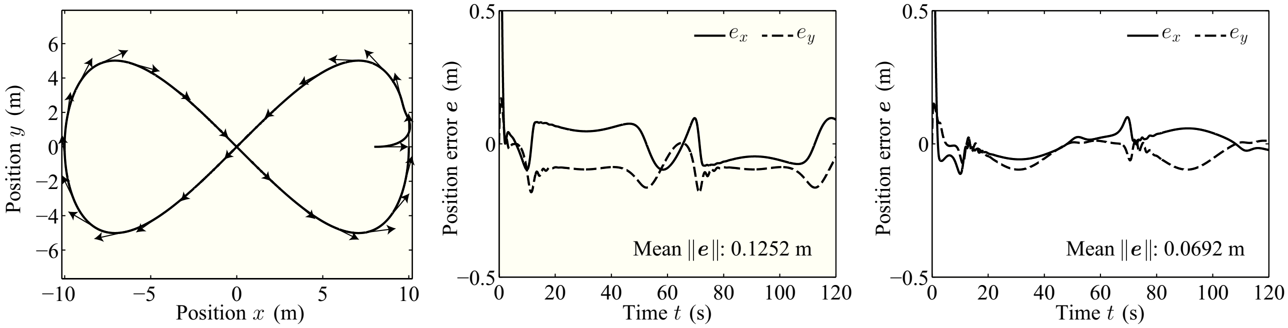

(a) Trajectory in static environment (b) Position error without feedforward (c) Position error with feedforward

Fig. 6. Path following trajectory and position error with and without pressure feedforward.

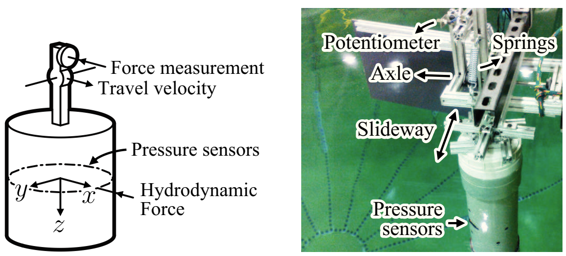

Fig. 7. Schematics and picture of the experiment setup.

fixed under a vertical beam along the z-axis, which is in turn pivoted about an axle in y-direction that translates along a horizontal track in x-direction. The cylinder is fully submerged under water with pressure sensors on the surface. At the other end of the beam, a spring structure and a linear potentiometer is installed to measure force. Scaled by the moment arm ratio, the force is compared to the pressure-based estimation.

Five ME755 160 kPa gauge sensors are arranged horizontally with equal intervals in the test. An MB1030 range sonar is used to register the position of the cylinder. In each run, the system starts from rest and accelerates to a constant speed before it decelerates back to a stop. The pressure distribution is assumed to be uniform along the vertical direction. Filtered and calibrated signals together with the force estimation are shown in Figs. 8 and 9. The estimated force generally captures the variations in the measurement, which verifies the algorithm. Note the mismatch between the signals may be due to the non-zero acceleration of the cylinder.

VI. Conclusion

In this paper, a lateral line inspired hydrodynamic force estimation for underwater vehicle control is expressed in three dimensional space and tested in simulation. A simple vehicle dynamic model may be resolved without considering the added mass and viscous damping terms. The feedforward element also contains hydrodynamic information about the surrounding background flow that is traditionally categorized as an unknown disturbance. Therefore, the pressure feedforward design may serve as an important guidance for control maneuvers especially in the presence of localization uncertainties and limited degrees of actuation. In agreement with this heuristic understanding, simulation results suggest an improvement in control performance. The force estimation algorithm is further verified with experimental tests.

Future work will be focusing on implementation of the pressure feedforward design in field tests. Moreover, the pressure distribution on the vehicle may also be influenced by propulsion, even though pressure measurements are excluded at locations of the actuators. As a result, information on the operation states of the actuators may be embedded in the signals, which potentially can be used as propulsion feedback.

References

[1] J. H. S. Blaxter, "Structure and development of the lateral line," *Biol. Rev.*, vol. 62, no. 4, pp. 471–514, Nov. 1987.

[2] H. Bleckmann, "Peripheral and central processing of lateral line information," *J. Comp. Physiol. A Neuroethol. Sens. Neural Behav. Physiol.*, vol. 194, no. 2, pp. 145–158, Feb. 2008.

[3] J. C. Montgomery, C. F. Baker, and A. G. Carton, "The lateral line can mediate rheotaxis in fish," *Nature*, vol. 389, pp. 960–963, Oct. 1997.

[4] T. J. Pitcher, B. L. Partridge, and C. S. Wardle, "A blind fish can school," *Science*, vol. 194, no. 4268, pp. 963–965, Nov. 1976.

[5] J. C. Montgomery and J. A. Macdonald, "Sensory tuning of lateral line receptors in Antarctic fish to the movements of planktonic prey," *Science*, vol. 235, no. 4785, pp. 195–196, Jan. 1987.

[6] K. Pohlmann, J. Atema, and T. Breithaupt, "The importance of the lateral line in nocturnal predation of piscivorous catfish," *J. Exp. Biol.*, vol. 207, pp. 2971–2978, Aug. 2004.

[7] S. Coombs, C. B. Braun, and B. Donovan, "The orienting response of Lake Michigan mottled sculpin is mediated by canal neuromasts," *J. Exp. Biol.*, vol. 204, pp. 337–348, Jan. 2001.

[8] M. Satou, H. A. Takeuchi, J. Nishii, M. Tanabe, S. Kitamura, N. Okumoto, and M. Iwata, "Behavioral and electrophysiological evidences that the lateral line is involved in the inter-sexual vibrational communication of the himé salmon (landlocked red salmon, *Oncorhynchus nerka*)," *J. Comp. Physiol. A Neuroethol. Sens. Neural Behav. Physiol.*, vol. 174, no. 5, pp. 539–549, May 1994.

[9] A. B. Kroese, J. M. van der Zalm, and J. van den Bercken, "Frequency response of the lateral-line organ of *Xenopus laevis*," *Pflugers Arch.*, vol. 375, no. 2, pp. 167–175, Jul. 1978.

[10] A. B. Kroese and N. A. Schellart, "Velocity- and acceleration-sensitive units in the trunk lateral line of the canal," *J. Neurophysiol.*, vol. 68, no. 6, pp. 2212–2221, Dec. 1992.

[11] Z. Fan, J. Chen, J. Zou, D. Bullen, C. Liu, and F. Delcomyn, "Design and fabrication of artificial lateral line flow sensors," *J. Micromech. Microeng.*, vol. 12, no. 5, pp. 655–661, Jun. 2002.

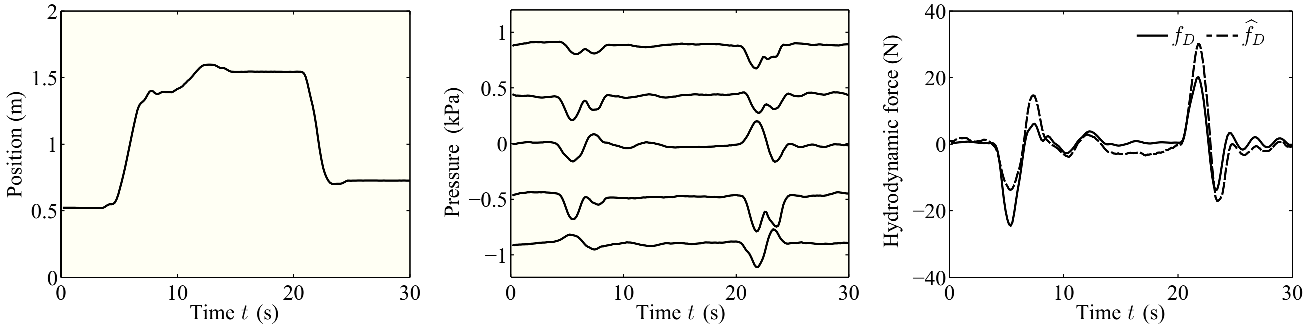

(a) Cylinder position (b) Pressure signals (c) Hydrodynamic force and its estimation

Fig. 8. Filtered signals and force estimation in experimental test 1.

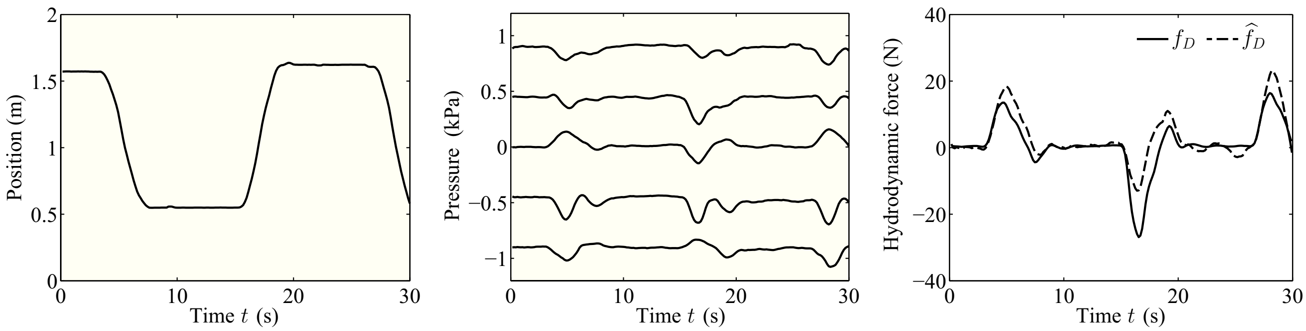

(a) Cylinder position (b) Pressure signals (c) Hydrodynamic force and its estimation

Fig. 9. Filtered signals and force estimation in experimental test 2.

[12] Y. Yang, J. Chen, J. Engel, S. Pandya, N. Chen, C. Tucker, S. Coombs, D. L. Jones, and C. Liu, "Distant touch hydrodynamic imaging with an artificial lateral line," in *Proc. Natl. Acad. Sci. USA*, vol. 103, no. 50, 2006, pp. 18 891–18 895.

[13] V. I. Fernandez, A. Maertens, F. M. Yaul, J. Dahl, J. H. Lang, and M. S. Triantafyllou, "Lateral-line-inspired sensor arrays for navigation and object identification," *Mar. Technol. Soc. J.*, vol. 45, no. 4, pp. 130–146, Jul./Aug. 2011.

[14] R. Venturelli, O. Akanyeti, F. Visentin, J. Ježov, L. D. Chambers, G. Toming, J. Brown, M. Kruusmaa, W. M. Megill, and P. Fiorini, "Hydrodynamic pressure sensing with an artificial lateral line in steady and unsteady flows," *Bioinspir. Biomim.*, vol. 7, no. 3, pp. 1–12, Apr. 2012.

[15] O. Akanyeti, L. D. Chambers, J. Ježov, J. Brown, R. Venturelli, M. Kruusmaa, W. M. Megill, and P. Fiorini, "Self-motion effects on hydrodynamic pressure sensing: Part I. Forward-backward motion," *Bioinspir. Biomim.*, vol. 8, pp. 1–10, Mar. 2013.

[16] Y. Xu, Z. Ren, and K. Mohseni, "Lateral line inspired pressure feedforward for autonomous underwater vehicle control," in *IEEE/RSJ IROS Workshop on Robotics for Environmental Monitoring*, Vilamoura, Algarve, Portugal, Oct. 2012, pp. 1–6.

[17] Y. Xu and K. Mohseni, "Bioinspired hydrodynamic force feedforward for autonomous underwater vehicle control," *IEEE/ASME Trans. Mechatronics*, 2013, submitted for publication.

[18] T. I. Fossen, *Guidance and Control of Ocean Vehicles*. New York, NY, USA: Wiley, 1994.

[19] M. Krieg, P. Klein, R. Hodgkinson, and K. Mohseni, "A hybrid class underwater vehicle: Bioinspired propulsion, embedded system, and acoustic communication and localization system," *Mar. Technol. Soc. J.*, vol. 45, no. 4, pp. 153–164, Jul./Aug. 2011.

[20] K. Mohseni, "Zero-mass pulsatile jets for unmanned underwater vehicle maneuvering," in *3rd AIAA Unmanned Unlimited Tech. Conf., Workshop Exhib.*, Chicago, IL, USA, Sep. 2004.

[21] ——, "Pulsatile vortex generators for low-speed maneuvering of small underwater vehicles," *Ocean. Eng.*, vol. 33, no. 16, pp. 2209–2223, Nov. 2006.

[22] T. M. Thomas, M. Krieg, and K. Mohseni, "Thrust characterization for bio-inspired pulsatile vortex ring thrusters with variable exit nozzle diameter," in *ASME Int. Mech. Eng. Congr. Expo.*, Buena Vista, FL, USA, Nov. 2009.

[23] M. Krieg and K. Mohseni, "Thrust characterization of pulsatile vortex ring generators for locomotion of underwater robots," *IEEE J. Ocean. Eng.*, vol. 33, no. 2, pp. 123–132, Apr. 2008.

[24] ——, "Dynamic modeling and control of biologically inspired vortex ring thrusters for underwater robot locomotion," *IEEE Trans. Robot.*, vol. 26, no. 3, pp. 542–554, Jun. 2010.

[25] L. A. Piegl and W. Tiller, *The NURBS Book*. New York, NY, USA: Springer-Verlag, 1997.

[26] D. F. Rogers, *An Introduction to NURBS: With Historical Perspective*. San Mateo, CA, USA: Morgan Kaufmann, 2001.

[27] R. A. Horn and C. R. Johnson, *Topics in Matrix Analysis*. Cambridge, U.K.: Cambridge Univ. Press, 1991.

[28] J. L. Buchanan and P. R. Turner, *Numerical Methods and Analysis*. New York, NY, USA: McGraw-Hill, 1992.

[29] J. D. Hoffman and S. Frankel, *Numerical Methods for Engineers and Scientists*, 2nd ed. New York, NY, USA: Marcel Dekker, 2001.

[30] Z. Ren, D. Hall, and K. Mohseni, "A hybrid pseudo-spectral immersed-boundary method for applications to aquatic locomotion," in *42nd AIAA Fluid Dynamics Conf.*, vol. 56, no. 18, New Orleans, LA, USA, Jun. 2012.

[31] X. Xia and K. Mohseni, "Axisymmetric synthetic jets: A momentum-based modeling approach," in *42nd AIAA Fluid Dynamics Conf.*, vol. 56, no. 18, New Orleans, LA, USA, Jun. 2012.

[32] Z. Qu and J. Xu, "Model-based learning controls and their comparisons using Lyapunov direct method," *Asian J. Control*, vol. 4, no. 1, pp. 99–110, Mar. 2002.

[33] B. Xian, D. M. Dawson, M. S. de Queiroz, and J. Chen, "A continuous asymptotic tracking control strategy for uncertain nonlinear systems," *IEEE Trans. Autom. Control*, vol. 49, no. 7, pp. 1206–1211, Jul. 2004.

[34] P. M. Patre, W. MacKunis, M. Johnson, and W. E. Dixon, "Composite adaptive control for Euler-Lagrange systems with additive disturbances," *Automatica*, vol. 46, no. 1, pp. 140–147, 2010.

[35] H. K. Khalil, *Nonlinear Systems*, 3rd ed. Englewood Cliffs, NJ, USA: Prentice-Hall, 2002.